Biogeosciences Discuss., 12, 17913–17951, 2015
www.biogeosciences-discuss.net/12/17913/2015/
doi:10.5194/bgd-12-17913-2015

Biogeosciences Discussions
Open Access
EGU

Methane and sulfate dynamics in sediments from mangrove-dominated tropical coastal lagoons, Yucatán, Mexico

P.-C. Chuang[1], M. B. Young[2], L. G. Miller[2], J. A. Herrera-Silveira[3], and A. Paytan[1,4]

[1]Department of Earth and Planetary Sciences, University of California Santa Cruz, 1156 High St., Santa Cruz, CA 95064, USA
[2]US Geological Survey, 345 Middlefield Rd, MS 434, Menlo Park, CA 94025, USA
[3]CINVESTAV-IPN, Unidad Mérida, A.P. 73 CORDEMEX, Mérida, Yucatán, Mexico
[4]Institute of Marine Sciences, University of California Santa Cruz, 1156 High St., Santa Cruz, CA 95064, USA

Received: 14 October 2015 – Accepted: 29 October 2015 – Published: 10 November 2015

Correspondence to: P.-C. Chuang (pchuan2@ucsc.edu)

Published by Copernicus Publications on behalf of the European Geosciences Union.

Abstract

Methane, sulfate and chloride concentrations in sediment porewater from two coastal mangrove ecosystems (Celestún and Chelem Lagoons) on the Yucatán Peninsula, Mexico were measured. In these sediments methane exists in shallow sediments where sulfate is not depleted, and sulfate reduction is actively occurring. A transport-reaction model depicting the various production and consumption processes for methane and sulfate is used to elucidate processes responsible for this observation. The model illustrates that methane in the upper sediments is produced in-situ supported by high dissolved organic matter as well as by non-competitive substrates. In addition methane is contributed to porewater in the upper sediments, where sulfate reduction occurs, by transport from deeper zones within the sedimentary column through bubbles dissolution and diffusion. The shallow methane production and accumulation depths in these sediments promote high methane fluxes to the water column and atmosphere.

1 Introduction

Wetlands are the largest natural source of methane (CH_4) to the atmosphere, accounting for between 20–25 % of the global atmospheric methane budget (Fung et al., 1991; Whalen, 2005). The primary source of this methane is microbial activity within anaerobic wetland sediments. Freshwater wetlands typically have much higher atmospheric methane fluxes than brackish to saline coastal areas (Bartlett et al., 1987, 1985), due primarily to the ability of sulfate-reducers to outcompete methanogens for shared substrates. Therefore saline and brackish sediments are characterized by either lower rates of methanogenesis, deeper zones of methanogenesis, or both (Holmer and Kristensen, 1994; Martens and Klump, 1984). Methane can be oxidized both aerobically and anaerobically within the sediments and water column, reducing emission to the atmosphere (Whalen, 2005). The depth at which methanogenesis occurs will determine

BGD
12, 17913–17951, 2015

the time of exposure to potential oxidizing conditions within the sediments, and can have a large effect on how much of the total methane produced is released from the sediments to the water column and atmosphere.

Despite brackish to marine salinities, high methane fluxes, comparable to those measured in freshwater wetlands, have been reported for coastal mangrove ecosystems in several places around the world, including Florida (Barber et al., 1988), Puerto Rico (Sotomayor et al., 1994), India (Biswas et al., 2004, 2007; Purvaja and Ramesh, 2000, 2001; Ramesh et al., 1997, 2007; Verma et al., 1999), Tanzania (Kristensen et al., 2008), Thailand (Lekphet et al., 2005), China (Alongi et al., 2005), Andaman Is. (Linto et al., 2014), Australia (Call et al., 2015) and the Yucatán Peninsula (Chuang et al., 2015). The anaerobic and organic-rich sediments found in mangrove ecosystems provide a suitable environment for methanogenesis, yet the extensive supply of sulfate from seawater should favor sulfate reducers over methanogens in the shallow sections of the sediments. There are, however, several possible ways that coastal wetland sediments can sustain relatively high methane fluxes despite high sulfate concentrations. If microbial activity of sulfate reducers is very high, sulfate may become rapidly depleted in the upper few centimeters of the sediment, allowing methanogens to dominate just below this zone. Additionally, methanogens can co-exist with sulfate reducers when noncompetitive substrates (those used only by methanogens and not by sulfate reducers) are available within the sediment. The mechanism of gas release from the sediment can also affect exposure time to oxidizing conditions in the sediment and may therefore have a significant effect on the total methane flux to the atmosphere. A large percentage of the methane produced in sediments is oxidized prior to reaching the atmosphere, and in shallow-water systems, the oxidation takes place primarily in the sediments and not in the water column (Martens and Klump, 1980). If enough methane builds up within the sediment, it can be released in the form of bubbles (ebullition), which can travel through the sediment and water column quickly, resulting in minimal oxidation (Barnes et al., 2006; Martens and Klump, 1980).

BGD
12, 17913–17951, 2015

The purpose of this study was to examine porewater methane distribution within the sediments of two mangrove-dominated coastal lagoons in Mexico in order to better understand the processes controlling methane flux from these sediments to the water column and atmosphere in these systems. By examining the spatial and temporal differences in porewater methane distributions at the mangrove lagoons, and relating them to sulfate concentrations and organic carbon content of the sediments, we can gain a better understanding of the factors controlling atmospheric methane flux from coastal mangrove ecosystems.

To do this we applied the transport-reaction model used in Wallmann et al. (2006) and Chuang et al. (2013) to simulate porewater profiles in order to understand factors controlling sources and sinks of porewater sulfate and methane and to assess rates of biogeochemical reactions in this dynamic system.

2 Study area

Sampling for this study was conducted in two mangrove-dominated coastal lagoons located on the western Yucatán Peninsula, Mexico (Fig. 1). The typical climatological pattern for this area consists of a dry season (March–May), a rainy season (June–October) during which the majority of the annual rainfall (> 500 mm) occurs, and the "nortes" season (November–February), which is characterized by moderate rainfall (20–60 mm) and intermittent high wind speeds greater than 80 km h^{-1} (Herrera-Silveira, 1994). Celestún Lagoon (20°52′ N, 90°22′ W) is long, narrow, and relatively shallow (average depth = 1.2 m). The inner and middle sections of the lagoon always have lower salinities than the section near the mouth due to year-round discharge of brackish groundwater from multiple submarine springs (Young et al., 2008). Salinity within the lagoon fluctuates seasonally, with salinity in the inner zone ranging from 8.9 to 18.2 during the course of this study, grading out to marine salinities at the mouth of the lagoon (Young et al., 2008).

BGD
12, 17913–17951, 2015

Celestún Lagoon is surrounded by 22.3 km^2 of well-developed mangrove forest, and has experienced relatively little disturbance from human development and/or pollution such as wastewater discharge (Herrera-Silveira et al., 1998). Sediments in Celestún consist primarily of autochthonous carbonate ooze. Chelem Lagoon (21°15′ N, 89°45′ W), in contrast, receives very little groundwater input and the area surrounding the lagoon has been heavily impacted by urban development. Salinity in Chelem ranges from brackish to hypersaline (24.8–40.3 during the study period), and vegetation surrounding the lagoon consists of scrub mangrove forest (Young et al., 2008). The construction of Yucalpeten Harbor in 1969 (Valdes and Real, 1998) increased circulation within the lagoon, and resulted in sandy marine sediments entering the lagoon. Sediments in Chelem deposited since 1969 consist of a heavily bioturbated mix of sands and autochthonous carbonate ooze, with a large number of shells of living and dead burrowing organisms (Valdes and Real, 1998).

3 Sampling and analytical methods

3.1 Porewater solutes and organic carbon content

Sediment cores were collected along lengthwise transects in both lagoons during the three different seasons. Sampling was conducted in Celestún and Chelem in April 2000 (dry season), December 2000 (nortes season), and October 2001 (late rainy season).

Sediments were sampled using hand-held acrylic push cores (7 cm inner diameter) either 30 or 60 cm in length. The push cores had holes drilled along the side at 2 cm intervals, which were sealed with electrical tape prior to sampling. Subsamples for porewater [CH_4] analysis were collected and methane concentrations were measured as described in (Chuang et al., 2015). After subsampling, the cores were capped, the holes were resealed, and the cores were transported back to the lab for sectioning and porewater extraction. In the laboratory, the cores were extruded and sliced into 2.5 cm depth intervals, then transferred into centrifuge tubes for porewater extraction. Core

BGD
12, 17913–17951, 2015

length was measured immediately after collection and just prior to extrusion in order to correct for compaction during transport.

Average compaction was 6 % of the total core length, and never exceeded 20 %. Porewater for sulfate (SO_4^{2-}) and chloride (Cl^-) analysis was extracted by centrifuging all the sediment from each depth interval to separate the porewater from the sediment, then passing the porewater through sterile 0.20 µm syringe filters inside an anaerobic chamber. Porewater samples were kept in 20 mL acid-cleaned glass scintillation vials and stored frozen until analysis.

Porewater [SO_4^{2-}] and [Cl^-] were measured by ion chromatography using a Dionex DX-500 IC equipped with an Ionpac AS9-HC column (4 mm) and AG9-HC (4 mm) guard column. The samples were diluted 5-fold with Milli-Q water prior to analysis in order to bring the [SO_4^{2-}] and [Cl^-] within the appropriate analytical range for the ion chromatograph. After porewater extraction, sediment samples were dried and prepared for analysis of organic carbon content ($C_{organic}$) as described in (Gonneea et al., 2004).

3.2 Sediment slurry incubation experiments

Sediment slurry incubations were performed in order to examine changes in methane production over different time intervals and at different substrate concentrations (Table 1). Incubations consisted of 3 competitive substrates (H_2, acetate, formate), 2 non-competitive substrates (methanol, trimethylamine (TMA)), and 4 types of controls. The controls (preparation methods are described below) consisted of an unammended sediment control under anaerobic conditions, an unammended aerobic control (partial oxygen headspace), a killed control in which the sediment was autoclaved to kill all living organisms in the sediment, and a chemical control in which biological methanogenesis was inhibited through the addition of 2-bromoethanesulfonic acid (BES) to a final concentration of 40 mM within the slurry. Triplicate bottles were prepared for each condition (controls and substrate additions), and methane headspace concentrations were measured at 3–4 time intervals over the course of 29 days.

BGD
12, 17913–17951, 2015

All the sediment slurries were prepared semi-anaerobically by homogenizing sediment in a blender with artificial seawater mixture in a 1 : 1 ratio under continuous flow of nitrogen gas. Large pieces of leaves, twigs, and shells were removed from the sediment prior to homogenization. 70 mL glass Wheaton bottles were flushed with nitrogen gas for 1 min prior to the addition of the sediment slurry. 30 mL of slurry was then added to each bottle under continuous nitrogen flow, and the bottles were sealed using blue butyl rubber stoppers and aluminum crimp seals. Substrate additions were made by injecting substrate solution into the bottle immediately after sealing the bottles, except for the H_2 gas treatment and the aerobic control. For the addition of H_2, the entire headspace of the bottles was flushed with 100 % H_2 gas. After each headspace sampling the H_2 gas removed by microbial activity in the sediment was replaced by inserting a gas tight syringe filled with 100 % H_2 gas into the bottles, and allowing the gas to be drawn into the bottles until equilibrium pressure was reached. The aerobic controls were prepared like the anaerobic, no amendment controls, except that 8 mL (20 % of the total headspace) of 100 % O_2 was added to the bottles immediately after they were sealed. In order to ensure that the sediment slurries remained aerobic, 100 % O_2 was added to the bottles throughout the incubation period. The sediment slurries were kept at room temperate (22 °C) and agitated continuously on a shaker table throughout the course of the incubations.

Headspace samples (0.25 mL) were extracted from the bottles at each time interval using a gas-tight syringe. Methane concentrations were measured on an HP 5730A gas chromatograph (GC) equipped with a flame ionization detector. GC calibration and creation of standard curves were based on successive dilutions of 100 % CH_4. Analytical error was approximately 5 % for CH_4 concentrations below 10 ppm-v (446 nM), and less than 3 % for CH_4 concentrations above 10 ppm-v as determined by repeat analyses of standards and samples.

BGD
12, 17913–17951, 2015

4 Results

4.1 Porewater concentrations of dissolved species

Representative porewater methane profiles reported in Chuang et al. (2015) are plotted alongside sulfate profiles in Fig. 2. Duplicate samples (1_1CH_Oct01 and 1_2CH_Oct01) were collected at station 1CH in Chelem lagoon. Porewater sulfate concentrations ranged from 0.21 to 35.3 mM in Celestún lagoon and from 4.13 to 33.5 mM in Chelem lagoon and show different trends (Fig. 2). In many of the cores higher sulfate is associated with lower methane particularly in cores located near the mouth of the lagoons (16CEL_Jul02, 16CEL_Oct01, 14CEL_Oct01, 14CEL_Jul02 and 5CH_Apr00) and lower sulfate with high methane in the inner zone of the lagoons (e.g. cores 1CEL_Jul02, 1CEL_Dec00, 3CEL_Jul02, 3CEL_Apr00, 1_1CH_Oct01, and 1_2 CH_Oct01).

The relationship between porewater salinity (represented by chloride concentration), porewater [CH_4], and porewater [SO_4^{2-}] appears to be spatially and temporally variable (Figs. 2 and 3). Higher sulfate is associated with higher chloride in cores located near the mouth of the lagoons and lower sulfate with lower chloride in the inner zone of the lagoons (Fig. 3a). Despite these general trends there are no clear consistent relationships between methane and chloride (Fig. 3b) and sulfate and methane (Fig. 3c) when all the data is considered together. The lack of consistent trends between chlorine (salinity), sulfate and methane in the cores suggest multiple processes impacting the distribution of these parameters, including physical processes such as mixing and dilution with seawater or groundwater and biological processes that are not sensitive to salinity such as sulfate reduction and methane production and oxidation. Specifically, brackish groundwater enters the lagoon through at least 30 subsurface discharge points (Young et al., 2008), and the chloride profiles suggest that some of this groundwater may seep through the sediments, resulting in localized decline in porewater salinities.

BGD
12, 17913–17951, 2015

To account for mixing with seawater and enable deciphering the physical and biological processes controlling the distribution of porewater solutes, observed sulfate depletion ($[SO_4^{2-}{}_{dep}]_{OBS}$) relative to seawater were calculated as the difference between the expected sulfate concentration contributed from seawater (determined based on porewater chloride analysis) and the measured sulfate concentration:

$$[SO_4^{2-}{}_{dep}]_{OBS} = \frac{[SO_4^{2-}]_{(SW)}}{[Cl^-]_{(SW)}} \times [Cl^-]_{(measured)} - [SO_4^{2-}]_{(measured)}, \quad (1)$$

where 0.05171 is applied for the $\frac{[SO_4^{2-}]_{(SW)}}{[Cl^-]_{(SW)}}$ ratio (Pilson, 1998).

Positive values indicate that sulfate has been removed from the porewater, most likely through sulfate reduction. Observed sulfate depletion when considered together with methane fall into five different trends (Fig. 2). In Group-1, sulfate depletion profiles show positive values (e.g. sulfate consumption or loss) with methane profiles mirroring the sulfate concentration profiles. The peaks for methane, sulfate and sulfate depletion are at the same depth. In Group-2, sulfate depletion is close to zero at surface depths and then increase with increasing depth which indicate sulfate input from the overlying water column and sulfate consumptions at depth. Methane concentrations for this group are scattered showing no relation to sulfate profiles. In Group-3, positive sulfate depletion values appear at the surface sediments and then decrease to almost zero at deeper depths. Methane profiles do not show strong relations with respect to sulfate depletion profiles in this group. In Group-4, the trend for sulfate depletion is similar to that of Group-3 with decreasing values toward the deeper sediment but starting from zero right at the surface. The negative sulfate depletion values and porwater sulfate concentrations above seawater values (> 28 mM) imply extra sulfate input from deeper depths. In Group-5, there is almost no sulfate depletion from the surface to the deeper depths and methane concentrations are low (< 0.25 mM) increasing from surface to deeper depths.

BGD
12, 17913–17951, 2015

4.2 Organic matter content

Representative sediment organic matter content profiles from each lagoon presented as dry weight percent organic carbon (DW% $C_{organic}$) are shown in Fig. 4. The profiles typically show a trend of increasing organic carbon content toward the deeper sections of the sediment. For example organic matter content varies from 0.06 % at the surface to 7 % at 15 cm in core 2CEL_Dec00. In cores 1CH_Oct01 and 1CH_Dec00 organic carbon decreases from 5 to 10 cm and then increased between 10 and 15 cm.

4.3 Sediment slurry incubation experiments

All the sediment slurries with added substrates showed increases in methane headspace concentrations significantly greater than those seen with either the no amendment aerobic and anaerobic controls or the treated controls (Fig. 5). The greatest increases in headspace [CH_4] were seen with additions of the two noncompetitive substrates, TMA and methanol. The H_2 treatment showed the next highest CH_4 production rate, followed by formate then acetate. Of the four control conditions, the no amendment, anaerobic treatment had the highest overall increase in headspace [CH_4]. The aerobic treatment had an initial higher increase in headspace [CH_4] than the no amendment, anaerobic treatment, although there was no detectable change in the headspace [CH_4] in the aerobic treatment between 150 and 700 h. Both the autoclaved and BES treatments did not show any changes in headspace [CH_4] greater than the instrumental detection limits.

5 Discussions

5.1 Co-existence of methane and sulfate in sediments

Seawater mixing through diffusion and irrigation into the sediment has clear effects on porewater solutes. Specifically the mixing results in dilution of the methane in the pore-

BGD
12, 17913–17951, 2015

water and enrichment of sulfate from seawater, hence masking any sulfate depletion values (e.g. rates of sulfate replenishments surpass sulfate reduction rates). This process is best seen near the mouth of the lagoon where low methane is associated with close to zero sulfate depletion. Negative sulfate depletion indicates mixing with water that is rich in sulfate relative to seawater and does not carry significant amounts of methane. Such conditions are seen primarily in the middle zone of Celestún Lagoon where groundwater springs input that is rich in sulfate due to anhydrite dissolution in the aquifer has been recorded (Perry et al., 2002, 2009). Positive sulfate depletion profiles occur at sites located in the inner zone of the lagoon suggesting significant sulfate reduction at rates higher than any replenishment from sulfate rich groundwater or seawater.

It is surprising that at some site particularly in the inner lagoon (1CEL, 2CEL, 3CEL and 1CH) high concentrations of methane and sulfate co-occur at the same depth in the sediment. This is not expected and not typically observed since methanogenesis and sulfate reduction do not tend to co-exist because sulfate reduction is more energetically favorable than methanogenesis and anaerobic oxidation of methane (AOM) coupled with sulfate reduction occurs in sulfate containing environments (Capone and Kiene, 1988; Valentine and Reeburgh, 2000). Previous research has shown that sulfate reducing microbes will out-compete methanogens for competitive substrates such as hydrogen and acetate, it is possible therefore that the high methane concentrations measured in sulfate rich porewater may be supplied by high rates of methanogenesis occurring at greater depths within the sediment below the sulfate reduction zone, or this may result from high abundance of competitive substrates in the sulfate reduction zone, hence reducing competition (Oremland and Polcin, 1982). The other possibility is that methanogens use various noncompetitive substrates (Oremland and Polcin, 1982; Wellsbury and Parkes, 2000). Indeed it has been reported that methanogens can use noncompetitive substrates, including methanol, trimethylamines and dimethylsulfide, in sulfate containing mangrove sediments and coastal lagoons (Lyimo et al., 2000; Mohanraju et al., 1997; Purvaja and Ramesh, 2001; Torres-Alvarado et al., 2013). Our

BGD
12, 17913–17951, 2015

sediment slurry incubation experiments demonstrated that in sediments from Celestún the methanogenic community is capable of producing methane from a wide range of substrates, including: H_2, acetate, formate, methanol, and trimethylamine (Fig. 5). Both methanol and trimethylamine are not utilized by sulfate reducers, which could allow methanogens to function at the same sediment depths as sulfate reducers (Fig. 5). The use of non-competitive substrates by the methanogenic community has important implications for methane flux to the atmosphere as it allows for methane production at shallow depths in the sediment reducing the potential for oxidation. Although processes and trends similar to those described above have been reported for other mangrove sediments the reports remain qualitative in nature. To better quantify the processes determining methane fluxes from mangrove sediments we use a transport-reaction model to simulate porewater data in these permanently submerged sediments.

5.2 Transport-reaction model setting and model results of methane and sulfate dynamics in mangrove sediments

In order to understand methane production and consumption and how these processes relate to sulfate dynamics in the lagoon sediments, we apply a transport-reaction model to simulate porewater data for profiles characterized by Group-1 and Group-2 trends where methane and sulfate co-occur (Fig. 2). Data for these two groups have positive net sulfate depletion rates indicative of sulfate reduction within the zone where methane concentrations are high. We also simulate net sulfate input and methane production/oxidation rates for data in Group-3, Group-4 and Group-5. Reactions considered in the model include organic matter (expressed as CH_2O in the equations below) degradation, organoclastic sulfate reduction (SR), methanogenesis, and anaerobic oxidation of methane (AOM). The following reactions are used for these processes:

Organoclastic sulfate reduction (SR):

$$2CH_2O + SO_4^{2-} \rightarrow 2HCO_3^- + H_2S \quad \text{(R1)}$$

BGD
12, 17913–17951, 2015

Methanogenesis:

$$2CH_2O \rightarrow CO_2 + CH_4 \quad \text{(R2)}$$

Anaerobic oxidation of methane (AOM):

$$CH_4 + SO_4^{2-} \rightarrow HCO_3^- + HS^- + H_2O \quad \text{(R3)}$$

The following equations were solved to quantify the rates of reaction and rates of transport of dissolved CH_4 and SO_4^{2-} and organic carbon (solid symbols; Fig. 4) in the upper 20 cm of the sediments (Berner, 1980; Boudreau, 1997):

$$\Phi \cdot \frac{\partial C}{\partial t} = \frac{\partial \left(\Phi \cdot D_s \cdot \frac{\partial C}{\partial x}\right)}{\partial x} - \frac{\partial (\Phi \cdot v \cdot C)}{\partial x} + \Phi \cdot R_c, \quad (2)$$

$$(1-\Phi) \cdot \frac{\partial G}{\partial t} = -\frac{\partial ((1-\Phi) \cdot w \cdot G)}{\partial x} + (1-\Phi) \cdot R_c, \quad (3)$$

where x is sediment depth, t is time, Φ is porosity, D_s is the solute-specific diffusion coefficient in the sediment, C is the concentration of solutes in the porewater, G is the organic content in dry sediment, v is the burial velocity of porewater, w is the burial velocity of solids, R_c is the sum of reactions. Sediment burial results in the downward movement of both sediment particles and porewater relative to the sediment water interface. Since we simulate $[SO_4^{2-}{}_{dep}]$ to derive organoclastic sulfate reduction rates and $[SO_4^{2-}{}_{dep}]$ is determined by seawater ($[Cl^-]$) any upward advection of fluids (typically low in Cl and high in sulfate) was not included in model. Solutes were simulated in moles L^{-1} of porewater (M) and organic contents in wt % (details of all the reaction terms and parameters are in Appendix).

Model derived $[SO_4^{2-}{}_{dep}]$, $[SO_4^{2-}]$ and $[CH_4]$ are shown in Fig. 2 by solid and dashed lines, respectively. Modeled porewater data in Group-1 sediments show that methane generated from active organic matter degradation within the upper sediments is more

BGD
12, 17913–17951, 2015

important than methane diffusing from below and gas bubble dissolution as seen in the sensitivity analysis from 1CEL_Jul02 and 2CEL_Jul02 (Fig. 6). In 1CEL_Jul02, gas dissolution of methane transported from deeper in the core does not need to be included in the model to achieve a good fit and in-situ methanogenesis alone can reproduce methane concentrations similar to the measured data. Indeed if we only consider gas dissolution without methanogenesis in the model for 1CEL_Jul02, the maximum methane that can be generated is not sufficient as depicted in the gray solid line because the maximum methane that can be dissolved from gas bubbles is 1.10 mM under the temperature, pressure and salinity of 1CEL_Jul02.

The modeled methane profile for 2CEL_Jul02 (black dashed line) requires the inclusion of methanogenesis (R_M), gas dissolution (R_{MB}) and anaerobic oxidation of methane (R_{AOM}). The black solid line represents only R_M and R_{AOM} in the simulation of methane. The gray solid and dashed lines represent only gas dissolution and R_{AOM} in the methane reaction terms (no methanogenesis within the modeled column (20 cm). The gray dashed line can fit methane concentrations below 10 cm depth and the gray solid line can fit methane concentrations in the upper 5 cm. Comparing results of the black solid and dashed lines, methanogenesis plus some gas dissolution are both needed for reproducing the methane distribution in core 2CEL_Jul02.

Table 2 lists the calculated depth-integrated turnover rates and fluxes for the individual modeled cores. Results for profiles in Group-1, methane sources include methanogenesis within the upper 20 cm and/or methane transported from deeper sections (> 20 cm) via bubble dissolution or diffusion. Methane can be supported fully by methanogenesis without gas bubble dissolution within the modeled upper 20 cm in cores 1CEL_Dec00, 1CEL_Jul02, 1_1CH_Oct01 and 1_2CH_Oct01. Gas bubble dissolution and transport from deeper sediments contributes more methane than methanogenesis in cores 1CEL_Apr00, 1CEL_Oct01, 2CEL_Dec00 and 3CEL_Jul02.

Methane sinks are AOM, methane emission to the water column or methane diffusion into deeper sediments (> 20 cm). Less than 5 % of methane was consumed by AOM showing that AOM is the minor sink for methane for cores in Group-1. The major sink

BGD
12, 17913–17951, 2015

for methane is methane emission to the water column accounting for over 90 % of methane produced within the 20 cm sediment column (e.g. 1CEL_Apr00, 1CEL_Oct01, 3CEL_Apr00 and 3CEL_Jul02).

Sulfate sinks include organoclastic sulfate reduction and AOM, but AOM also plays a minor role for sulfate reduction. Organoclastic sulfate reduction, ranging from 1.1 to 24 mmol SO_4^{2-} m^{-2} d^{-1}, is the major sink for sulfate and organic carbon in most cores. If organoclastic sulfate reduction is converted to C units this process can account for 2.2–50 mmol C m^{-2} d^{-1} of inorganic C release; in the same range of that reported for most mangrove sediments (Kristensen et al., 2008). Specifically in this system there are indications for additional sulfate inputs to the porewater (low Cl high sulfate groundwater) hence the calculated net sulfate reaction rates ($F_{\text{sulfate (net)}}$) are underestimated of the actual reduction rates (e.g. cores 1CEL_Dec00, 1CEL_Oct01, 2CEL_Dec00 and 2CEL_Jul02).

Organoclastic sulfate reduction and methanogenesis derived from the rate of organic matter mineralization range from 3.4 to 113 mmol C m^{-2} d^{-1}. However, the organic matter content in the sediments increase with depth and accumulates in the deeper sediments, inconsistent with expected consumptions trends (Fig. 4). Organic carbon degradation rates for data in Fig. 4 were quantified by Eq. (A11). Results show negative values which means organic carbon accumulates and is buried in the deeper sediments (as observed) (Table 2). Organic carbon burial rates derived from the model for both lagoons (Table 2) are in the same range as those reported in Gonneea et al. (2004) (9–16 mmol C m^{-2} d^{-1} in Celestún Lagoon and 15–24 mmol C m^{-2} d^{-1} in Chelem Lagoon). The measured organic carbon content may contain high amount of refractory carbon yet the degradation rates (R_{POC}; Eq. A7) converted from sulfate depletion rates likely represent the more labile organic carbon pool which is no longer present in the sediment or dissolved organic matter which was not considered (or measured) in this study. A wide range of substrates, including: H_2, acetate, formate, methanol, and trimethylamine which are not included in the sedimentary organic matter measured in the core can be utilized for methane production and/or sulfate reduction (Fig. 2) the high cal-

BGD
12, 17913–17951, 2015

culated organic carbon oxidation rates are therefore not surprising. Indeed mangrove systems in general (e.g. Dittmar et al., 2006; Dittmar and Lara, 2001; Lee, 1995; Odum and Heald, 1975) and the lagoons in Yucatan in particular are dominated by high DOC (Young et al., 2005). Although the $(1 - f_{SO_4})$ term in Eq. (A8) may indicate that methanogenesis is inhabited by sulfate (R_M is from competitive substrates) it can also be explained as the portion of organic carbon degradation (R_M) from non-competitive substrates within the modeled length.

Methane concentrations are not reproduced as well for cores in Group-2 (in comparison to Group-1) in our model. No methanogenesis is seen in the upper sediments as suggested by the negative value of F_{SR}. Different combinations of methanogenesis and methane input from below are needed to explain the trends. For example gas dissolution is the major source of methane in core 1CH_Dec00, while methanogenesis and gas dissolution are both needed for core 1CH_Apr00. AOM is the major reaction in cores 2CH_Dec00 and 5CH_Apr00. Sensitivity analysis (Fig. 6) shows that methane concentrations in the model are much lower than the measured data (observations) gas dissolution is not included in 1CH_Apr00 and 1CH_Dec00. Model derived methane concentrations far exceed measured methane concentrations in 2CH_Dec00 and 5CH_Apr00 when methanogenesis is included which implies that organoclastic sulfate reduction takes place in these cores, but the availability of non-competitive/competitive substrates is too low above the 20 cm (Fig. 6). This may imply that other mechanisms in addition to methanogenesis, gas dissolution, or AOM affect methane concentrations in cores from this group. Such mechanisms may include high organic content of substrates such as DOC that support methane production and were not included in the methanogenesis term in cores 1CH_Dec00 and 1CH_Apr00 and methane degassing or dilution by low methane groundwater in cores 2CH_Dec00 and 5CH_Apr00.

Although sulfate depletion values for cores in Group-3 are positive, sulfate concentrations are high suggesting sulfate input from deeper sediments so that R_{SD} and R_{SR} are negative (Table 2). As noted before, this enrichment could be from sulfate rich

BGD
12, 17913–17951, 2015

groundwater flow (Perry et al., 2002, 2009; Young et al., 2008). Cores in Group-4 and Group-5 also show negative or zero sulfate depletion values and are most likely similar to cores in Group-3 for which methanogenesis rates and sulfate reduction rates are underestimated due to the low sulfate depletion (R_{SR}) estimates resulting from sulfate addition from groundwater.

Depth-integrated methane production or consumption rates (F_{CH_4}) and net sulfate inputs ($F_{SO_4^{2-}}$) calculated from Eqs. (A12) and (A13) for cores in Group-3, Group-4 and Group-5 are listed in Table 2. Methane and sulfate net production/consumption rates ranged from 0.012–11 mmol $CH_4\,m^{-2}\,d^{-1}$ and 0.83–10 mmol $SO_4^{2-}\,m^{-2}\,d^{-1}$. Negative values indicate net sulfate or methane consumptions. AOM plays a minor role in cores in Group-3, Group-4 and Group-5 like in Groups 1 and 2. Although specific sources of methane and sulfate can not be identified using this approach independent studies suggest that sulfate can be added from external sources specifically groundwater in this region (Gonneea et al., 2014; Perry et al., 2009, 2002; Young et al., 2008). The major sink for methane in these cores is methane emission to the water.

6 Conclusions

The variable trends observed in porewater chemistry indicate a very dynamic system and can be explained by different rates of operation of physical processes such as mixing and dilution with seawater or groundwater and biological processes (bacterial methane production and methane and sulfate consumption). Although organic carbon degradation rates are dominated by organoclastic sulfate reduction in these cores methanogenesis both in shallow and deeper sediments is prevalent. The co-occurrence of methane and sulfate reduction (documented by sulfate depletion) in shallow sediments in this system is explained by high methane production rates supported by non-competitive substrates and ample dissolved and labile organic matter in the shallow sediments as well as the contributions of methane from deeper sediment through bubbles dissolution and diffusion. AOM is a minor sink for sulfate and

BGD
12, 17913–17951, 2015

methane. The major sink for methane is methane efflux to the water column. Build-up of methane at shallow depths may reduce the fraction of methane that is oxidized prior to entering the water column, thereby increasing the flux to the atmosphe, and it may also encourage methane flux through bubble release, which can also result in a larger fraction of the methane produced reaching the atmosphere without being lost to oxidation. Specifically, the ability of the microbial community in these sediments to use non-competitive substrates may contribute to the higher than expected atmospheric methane flux measured from these mangrove lagoons.

Appendix: Modeling procedure used in the evaluation of the mangrove-dominated tropical coastal lagoons, Yucatán, Mexico data

Details of the modeling procedure and parameters are described in the following equations and Tables A1–A3. In Eqs. (2) and (3), sediment porosity decreases with depth due to steady-state compaction:

$$\Phi = \Phi_f + (\Phi_0 - \Phi_f) \cdot e^{-px}, \quad \text{(A1)}$$

where Φ_f is porosity below the depth of compaction (0.78 for Celestún and 0.83 for Chelem), Φ_0 is porosity at the sediment surface (0.90 for Celestún and 0.89 for Chelem) and p ($1/15\,\mathrm{cm}^{-1}$) is the depth attenuation coefficient of porosity. These parameters were determined from the measured porosity data at each site or nearby site.

Under the assumption of steady state compaction, the advection of fluids was calculated as in (Wallmann et al., 2006):

$$v = \frac{\phi_f \cdot w_f}{\phi}, \quad \text{(A2)}$$

$$w = \frac{(1-\phi_f) \cdot w_f}{(1-\phi)}, \quad \text{(A3)}$$

BGD
12, 17913–17951, 2015

where w_f is the sedimentation rate of compacted sediments calculated from ^{210}Pb dating of sediments (0.25 cm yr^{-1} for Celestún and 0.35 cm yr^{-1} for Chelem; Gonneea et al., 2004).

The sediment diffusion coefficient of each solute (D_s) was calculated according to Archie's law considering the effect of tortuosity on diffusion (Boudreau, 1997):

$$D_s = \Phi^2 \cdot D_M, \quad \text{(A4)}$$

where D_M is the molecular diffusion coefficient at the in situ temperature, salinity and pressure (Table A1) calculated according to (Boudreau, 1997). The net reaction terms (R_C in Eq. A2) of modeled species are given in Table A2 and boundary conditions used in the model are listed in Table A3.

Since net sulfate consumption is observed in Groups 1 and 2 profiles (Fig. 2). We use the following calculations to obtain sulfate depletion rates (R_{SD}) which are set to be proportional to the difference between modeled $\left(C\left(SO_{4\ dep}^{2-}\right)\right)$ and measured concentrations $\left(C\left(SO_{4\ dep}^{2-}\right)_{OBS}\right)$. The corresponding kinetic constant is set to be high (k_{SD} = 100–500 y^{-1}) so that concentrations calculated in the model are always very close to measured values.

$$R_{SD} = k_{SD} \cdot \left(C\left(SO_{4\ dep}^{2-}\right)_{OBS} - C\left(SO_{4\ dep}^{2-}\right)\right) \quad \text{(A5)}$$

In Wallmann et al. (2006), Michaelis–Menten kinetic limitation terms were used to define how the rate of organic carbon degradation (R_{POC}) is coupled to rate of organoclastic sulfate reduction (R_{SR}) and methanogenesis (R_M). R_{SR} is obtained by Eq. (A5) for sites where $[SO_{4\ dep}^{2-}]_{OBS}$ is positive. Since AOM may play a minor role in the methane and sulfate rich sediment and R_{AOM} was included in the net reaction rates of methane and sulfate this is justified.

$$R_{SR} = R_{SD} \quad \left(C\left(SO_{4\ dep}^{2-}\right)_{OBS} > 0\right) \quad \text{(A6)}$$

BGD
12, 17913–17951, 2015

Though organic carbon profiles were not simulated in this study due to limited measured data (data available only for a few cores), R_{POC} can be obtained via the Michaelis–Menten kinetic limitation term:

$$R_{POC} = \frac{R_{SR}}{0.5 \cdot f_C \cdot f_{SO_4^{2-}}}, \quad \text{(A7)}$$

where $f_{SO_4^{2-}} = \frac{C_{SO_4^{2-}}}{C_{SO_4^{2-}} + k_{SR}}$ is the Michaelis–Menten rate-limiting term for sulfate reduction, k_{SR} is the Michaelis–Menten kinetic constant for organoclastic sulfate reduction (in mM), $f_C = \frac{ds \times (1-\Phi) \times 10}{MW_C \times \Phi}$ is the factor used to convert between solid and dissolved species concentrations, where MW_C is the molecular weight of carbon ($12\,g\,mol^{-1}$) and ds is the density of dry solids ($2.5\,g\,cm^{-3}$) (Wallmann et al., 2006), Michaelis–Menten kinetic limitation term used for methanogenesis (R_M) is expressed as:

$$R_M = 0.5 \cdot f_C \cdot R_{POC} \cdot (1 - f_{SO_4^{2-}}). \quad \text{(A8)}$$

The rate of AOM (R_{AOM}) was simulated using bimolecular kinetics (Regnier et al., 2011):

$$R_{AOM} = k_{AOM} \cdot C_{CH_4} \cdot C_{SO_4^{2-}}, \quad \text{(A9)}$$

where k_{AOM} is kinetic constant for R_{AOM} ($20\,yr^{-1}\,M^{-1}$). Since gas bubbles were observed in the field and ebullition fluxes were measureable by floating chambers (Chuang et al., 2015), dissolution of the gas bubbles rising through the sediment was considered to occur:

$$CH_{4(g)} \rightarrow CH_4 \quad \text{if } CH_4 \leq L_{MB} \quad \text{(R4)}$$

Methane dissolution (R_{MB}):

$$R_{MB} = k_{MB} \cdot \left(L_{MB} - C_{CH_4}\right) \quad \text{(A10)}$$

BGD
12, 17913–17951, 2015

where L_{MB} is the in situ methane gas solubility concentration (Haeckel et al., 2004) calculated using the algorithm of (Duan et al., 1992a and b) and the site-specific salinity, temperature and pressure of the bottom water. The rate of gas dissolution (R_{MB}) depends on the difference between L_{MB} and the in situ methane concentration using a first-order rate constant k_{MB}. k_{MB} is a fitting parameter that lumps together the rate of gas dissolution in addition to diffusion of dissolved gas in the bubble tubes and walls.

We use the same approach as that used for obtaining sulfate depletion rates (R_{SD}) to calculate organic carbon degradation ($C_{organic}$) rates in cores 2CEL_Dec00, 3CEL_Dec00, 1CH_Dec00 and 1CH_Oct01 (Fig. 4) where organic carbon data is available.

$$R_{C_{organic}} = k_{C_{organic}} \cdot (C_{organic_{OBS}} - C_{organic}) \quad \text{(A11)}$$

Organic carbon degradation rates ($R_{C_{organic}}$) are set to be proportional to the difference between modeled ($C_{organic}$) and measured concentrations ($C_{organic_{OBS}}$). The corresponding kinetic constant $k_{C_{organic}}$ is 0.01 yr^{-1}.

Net methane and sulfate reaction rates for porewater data in Group-3, Group-4 and Group-5 are expressed as:

$$R_{CH_4} = k_{CH_4} \cdot \left(C_{CH_4 OBS} - C_{CH_4}\right), \quad \text{(A12)}$$

$$R_{SO_4^{2-}} = k_{SO_4^{2-}} \cdot \left(C_{SO_4^{2-}\,OBS} - C_{SO_4^{2-}}\right). \quad \text{(A13)}$$

In Eqs. (A12) and (A13), methane and sulfate rates (R_{CH_4} and $R_{SO_4^{2-}}$) are set to be proportional to the difference between modeled (C_{CH_4} and $C_{SO_4^{2-}}$) and measured concentrations ($C_{CH_4 OBS}$ and $C_{SO_4{}^{2-}\,OBS}$). The corresponding kinetic constant k_{CH_4} and $k_{SO_4{}^{2-}}$ are listed in Table A1. AOM rates are estimated via Eq. (A9) by using the modeled methane and sulfate concentrations from Eqs. (A12) and (A13).

Fixed concentrations were imposed for all solutes at the upper and lower boundaries which were set to values measured at or near the sediment–water interface and at

BGD
12, 17913–17951, 2015

20 cm. The method–of–lines was used to transfer the set of finite difference equations of the spatial derivatives of the coupled partial differential equations to the ordinary differential equation solver (NDSolve) in MATHEMATICA v. 7.0. All models were run for 1×10^6 yr to achieve steady state using a grid spacing which increased from ca. 0.015 cm at the sediment surface to 0.38 cm at depth. Mass balance was typically better than 99.5 %.

Acknowledgements. We thank the staff of the DUMAC Celestún station and the students of CINVESTAV for assistance with laboratory space, lodging, and field work. We thank Tom Lorenson and Ron Oremland of the Menlo Park, CA USGS for facility use and analyses. This work was funded by Consejo Nacional de Ciencia y Tecnología Ref: 4147-P T9608, 32356T, and CONABIO Ref: B019 to J H-S, NSF INT 009214214 to AP, and a Stanford Graduate Fellowship and Lieberman Fellowship to M. B. Young.

References

Alongi, D. M., Pfitzner, J., Trott, L. A., Tirendi, F., Dixon, P., and Klumpp, D. W.: Rapid sediment accumulation and microbial mineralization in forests of the mangrove Kandelia candel in the Jiulongjiang Estuary, China, Estuar. Coast. Shelf S., 63, 605–618, 2005.

Barber, T. R., Burke, R. A., and Sackett, W. M.: Diffusive flux of methane from warm wetlands, Global Biogeochem. Cy., 2, 411–425, 1988.

Barnes, J., Ramesh, R., Purvaja, R., Nirmal Rajkumar, A., Senthil Kumar, B., Krithika, K., Ravichandran, K., Uher, G., and Upstill-Goddard, R.: Tidal dynamics and rainfall control N_2O and CH_4 emissions from a pristine mangrove creek, Geophys. Res. Lett., 33, L15405, doi:10.1029/2006GL026829, 2006.

Bartlett, K. B., Harriss, R. C., and Sebacher, D. I.: Methane flux from coastal salt marshes, J. Geophys. Res.-Atmos., 90, 5710–5720, 1985.

Bartlett, K. B., Bartlett, D. S., Harriss, R. C., and Sebacher, D. I.: Methane emissions along a salt marsh salinity gradient, Biogeochemistry, 4, 183–202, 1987.

Berner, R. A.: Early Diagenesis. A Theoretical Approach, Princeton University Press, Princeton, NJ, USA, 241 pp., 1980.

BGD
12, 17913–17951, 2015

Biswas, H., Mukhopadhyay, S. K., De, T. K., Sen, S., and Jana, T. K.: Biogenic controls on the air-water carbon dioxide exchange in the Sundarban mangrove environment, northeast coast of Bay of Bengal, India, Limnol. Oceanogr., 49, 95–101, 2004.

Biswas, H., Mukhopadhyay, S. K., Sen, S., and Jana, T. K.: Spatial and temporal patterns of methane dynamics in the tropical mangrove dominated estuary, NE coast of Bay of Bengal, India, J. Marine Syst., 68, 55–64, 2007.

Boudreau, B. P.: Diagenetic Models and Their Implementation: Modelling Transport and Reactions in Aquatic Sediments, Springer-Verlag, Berlin, 414 pp., 1997.

Call, M., Maher, D. T., Santos, I. R., Ruiz-Halpern, S., Mangion, P., Sanders, C. J., Erler, D. V., Oakes, J. M., Rosentreter, J., Murray, R., and Eyre, B. D.: Spatial and temporal variability of carbon dioxide and methane fluxes over semi-diurnal and spring–neap–spring timescales in a mangrove creek, Geochim. Cosmochim. Ac., 150, 211–225, 2015.

Capone, D. G. and Kiene, R. P.: Comparison of microbial dynamics in marine and freshwater sediments: contrasts in anaerobic carbon catabolism1, Limnol. Oceanogr., 33, 725–749, 1988.

Chuang, P.-C., Dale, A. W., Wallmann, K., Haeckel, M., Yang, T. F., Chen, N.-C., Chen, H.-C., Chen, H.-W., Lin, S., Sun, C.-H., You, C.-F., Horng, C.-S., Wang, Y., and Chung, S.-H.: Relating sulfate and methane dynamics to geology: accretionary prism offshore SW Taiwan, Geochem. Geophy. Geosy., 14, 2523–2545, 2013.

Dittmar, T. and Lara, R. J.: Driving forces behind nutrient and organic matter dynamics in a mangrove tidal creek in North Brazil, Estuar. Coast. Shelf S., 52, 249–259, 2001.

Dittmar, T., Hertkorn, N., Kattner, G., and Lara, R. J.: Mangroves, a major source of dissolved organic carbon to the oceans, Global Biogeochem. Cy., 20, GB1012, doi:10.1029/2005GB002570, 2006.

Duan, Z., Møller, N., Greenberg, J., and Weare, J. H.: The prediction of methane solubility in natural waters to high ionic strength from 0 to 250 °C and from 0 to 1600 bar, Geochim. Cosmochim. Ac., 56, 1451–1460, 1992a.

Duan, Z. H., Møller, N., and Weare, J. H.: An equation of state for the CH_4-CO_2-H_2O system.1. pure systems from 0 °C to 1000 °C And 0 to 8000 bar, Geochim. Cosmochim. Ac., 56, 2605–2617, 1992b.

Fung, I., John, J., Lerner, J., Matthews, E., Prather, M., Steele, L. P., and Fraser, P. J.: Three-dimensional model synthesis of the global methane cycle, J. Geophys. Res.-Atmos., 96, 13033–13065, 1991.

BGD
12, 17913–17951, 2015

Gonneea, M. E., Paytan, A., and Herrera-Silveira, J. A.: Tracing organic matter sources and carbon burial in mangrove sediments over the past 160 years, Estuar. Coast. Shelf S., 61, 211–227, 2004.
Gonneea, M. E., Charette, M. A., Liu, Q., Herrera-Silveira, J. A., and Morales-Ojeda, S. M.: Trace element geochemistry of groundwater in a karst subterranean estuary (Yucatan Peninsula, Mexico), Geochim. Cosmochim. Ac., 132, 31–49, 2014.
Haeckel, M., Suess, E., Wallmann, K., and Rickert, D.: Rising methane gas bubbles form massive hydrate layers at the seafloor, Geochim. Cosmochim. Ac., 68, 4335–4345, 2004.
Herrera-Silveira, J .A.: Nutrients from udergrounds discharges in a coastal lagoon (Celestún, Yucatán, México), Verhandlungen des Internationalen Verein Limnologie, 25, 1398–1403, 1994.
Herrera-Silveira, J. A., Ramìrez R, J., and Zaldivar R, A.: Overview and characterization of the hydrology and primary producer communities of selected coastal lagoons of Yucatán, México, Aquatic Ecosystem Health and Management, 1, 353–372, 1998.
Holmer, M. and Kristensen, E.: Coexistence of sulfate reduction and methane production in an organic-rich sediment, Mar. Ecol.-Prog. Ser., 107, 177–184, 1994.
Kristensen, E., Bouillon, S., Dittmar, T., and Marchand, C.: Organic carbon dynamics in mangrove ecosystems: a review, Aquat. Bot., 89, 201–219, 2008.
Lee, S. Y.: Mangrove outwelling – a review, Hydrobiologia, 295, 203–212, 1995.
Lekphet, S., Nitisoravut, S., and Adsavakulchai, S.: Estimating methane emissions from mangrove area in Ranong Province, Thailand, Songklanakarin, J. Sci. Technol., 27, 153–163, 2005.
Linto, N., Barnes, J., Ramachandran, R., Divia, J., Ramachandran, P., and Upstill-Goddard, R. C.: Carbon dioxide and methane emissions from mangrove-associated waters of the Andaman islands, Bay of Bengal, Estuar. Coast., 37, 381–398, 2014.
Lyimo, T. J., Pol, A., den Camp, H. J. M., Harhangi, H. R., and Vogels, G. D.: Methanosarcina semesiae sp nov., a dimethylsulfide-utilizing methanogen from mangrove sediment, Int. J. Syst. Evol. Micr., 50, 171–178, 2000.
Martens, C. S. and Klump, V. J.: Biogeochemical cycling in an organic-rich coastal marine basin.1. Methane sediment-water exchange processes, Geochim. Cosmochim. Ac., 44, 471–490, 1980.

BGD
12, 17913–17951, 2015

Martens, C. S. and Klump, V. J.: Biogeochemical cycling in an organic-rich coastal marine basin 4. An organic carbon budget for sediments dominated by sulfate reduction and methanogenesis, Geochim. Cosmochim. Ac., 48, 1987–2004, 1984.

Mohanraju, R., Rajagopal, B. S., and Daniels, L.: Isolation and characterization of a methanogenic bacterium from mangrove sediments, J. Mar. Biotechnol., 5, 147–152, 1997.

Odum, W. E. and Heald, E. J.: The detritus-based food web of an estuarine mangrove community, in: Estuarine Research, edited by: Cronin, L. E., New York, Academic Press, Inc., 265–286, 1975.

Oremland, R. S. and Polcin, S.: Methanogenesis and sulfate reduction – competitive and noncompetitive substrates in estuarine sediments, Appl. Environ. Microb., 44, 1270–1276, 1982.

Perry, E., Velazquez-Oliman, G., and Marin, L.: The hydrogeochemistry of the karst aquifer system of the northern Yucatan Peninsula, Mexico, Int. Geol. Rev., 44, 191–221, 2002.

Perry, E., Paytan, A., Pedersen, B., and Velazquez-Oliman, G.: Groundwater geochemistry of the Yucatan Peninsula, Mexico: constraints on stratigraphy and hydrogeology, J. Hydrol., 367, 27–40, 2009.

Pilson, M. E. Q.: An Introduction to the Chemistry of the Sea, Prentice Hall, Upper Saddle River, New Jersey, 431 pp., 1998.

Purvaja, R. and Ramesh, R.: Human impacts on methane emission from mangrove ecosystems in India, Reg. Environ. Change, 1, 86–97, 2000.

Purvaja, R. and Ramesh, R.: Natural and anthropogenic methane emission from coastal wetlands of South India, Environ. Manage., 27, 547–557, 2001.

Ramesh, R., Purvaja, G. R., Parashar, D. C., Gupta, P. K., and Mitra, A. P.: Anthropogenic forcing on methane efflux from polluted wetlands (Adyar River) of Madras City, India, Ambio, 26, 369–374, 1997.

Ramesh, R., Purvaja, R., Neetha, V., Divia, J., Barnes, J., and Upstill-Goddard, R.: CO_2 and CH_4 emissions from Indian mangroves and its surrounding waters, in: Greenhouse gas and carbon balances in mangrove coastal ecosystems, Proceedings, edited by: Tateda, Y., Gendai Tosho, Kanagawa, Japan, 153–164, 2007.

Regnier, P., Dale, A. W., Arndt, S., LaRowe, D. E., Mogollon, J., and Van Cappellen, P.: Quantitative analysis of anaerobic oxidation of methane (AOM) in marine sediments: a modeling perspective, Earth-Sci. Rev., 106, 105–130, 2011.

Sotomayor, D., Corredor, J. E., and Morell, J. M.: Methane flux from mangrove sediments along the southwestern coast of Puerto-Rico, Estuaries, 17, 140–147, 1994.

BGD
12, 17913–17951, 2015

Torres-Alvarado, M., José Fernández, F., Ramírez Vives, F., and Varona-Cordero, F.: Dynamics of the methanogenic archaea in tropical estuarine sediments, Archaea, 13, 582646, doi:10.1155/2013/582646, 2013.
Valdes, D. S. and Real, E.: Variations and relationships of salinity, nutrients and suspended solids in Chelem coastal lagoon at Yucatan, Mexico, Indian J. Mar. Sci., 27, 149–156, 1998.
Valentine, D. L. and Reeburgh, W. S.: New perspectives on anaerobic methane oxidation, Environ. Microbiol., 2, 477–484, 2000.
Verma, A., Subramanian, V., and Ramesh, R.: Day-time variation in methane emission from two tropical urban wetlands in Chennai, Tamil Nadu, India, Curr. Sci. India, 76, 1020–1022, 1999.
Wallmann, K., Aloisi, G., Haeckel, M., Obzhirov, A., Pavlova, G., and Tishchenko, P.: Kinetics of organic matter degradation, microbial methane generation, and gas hydrate formation in anoxic marine sediments, Geochim. Cosmochim. Ac., 70, 3905–3927, 2006.
Wellsbury, P. and Parkes, R. J.: Deep biosphere: source of methane for oceanic hydrate, in: Natural gas hydrate in oceanic and permafrost environments, edited by: Max, M. D., Springer, New York, 91–104, 2000.
Whalen, S. C.: Biogeochemistry of methane exchange between natural wetlands and the atmosphere, Environ. Eng. Sci., 22, 73–94, 2005.
Young, M. B., Gonneea, M. E., Herrerasilveira, J. A., and Paytan, A.: Export of Dissolved and Particulate Carbon and Nitrogen From a Mangrove-Dominated Lagoon, Yucatán Peninsula, Mexico, Int. J. Ecol. Environ. Sci., 31, 189–202, 2005.
Young, M. B., Gonneea, M. E., Fong, D. A., Moore, W. S., Herrera-Silveira, J., and Paytan, A.: Characterizing sources of groundwater to a tropical coastal lagoon in a karstic area using radium isotopes and water chemistry, Mar. Chem., 109, 377–394, 2008.

BGD
12, 17913–17951, 2015

Table 1. Experimental conditions and sampling time intervals for methane headspace concentration analysis of sediment slurry incubations.

	Treatment	Initial concentration	Experiment length (days)	Number of measurements
Controls	No amendment (anaerobic)	N_2 headspace	29	3
	Autoclaved	N_2 headspace	29	3
	Aerobic- O_2 gas	16 % O2 headspace (0.36 mM)	29	3
	BES	40 mM	29	3
Competitive substrates	H_2 gas	100 % headspace (1.8 mM)	29	3
	Acetate	10 mM	29	3
	Formate	10 mM	29	3
Noncompetitive substrates	Methanol	10 mM	29	4
	TMA	10 mM	29	4

BGD
12, 17913–17951, 2015

Table 2. Depth-integrated turnover rates (mmol m^{-2} d^{-1}) and contributions of methanogenesis to net methane production (%) and organoclastic sulfate reduction to POC degradation (%).

	Length of model column (cm)	F_{SD}	F_M	F_{SR}	F_{POC}	F_{AOM}	F_{MB}	$F_{methane\ (top)}$	$F_{methane\ (bottom)}$	$F_M/(F_M+F_{MB})$	$2F_{SR}/F_{POC}$	$F_{C_{organic}}$	$F_{SO_4^{2-}}$	F_{CH_4}
Group-1														
1CEL_Apr00	20	3.7	0.13	3.7	8.1	0.017	0.41	0.59	0.06	25 %	92 %			
1CEL_Dec00	20	2.2	2.9	12	30	0.051	0	2.2	−0.65	100 %	77 %			
1CEL_Oct01	20	6.2	0.16	12	25	0.014	0.32	0.43	−0.03	33 %	96 %			
1CEL_Jul02	20	3.6	8.1	3.6	24	0.11	0	7.7	−1.97	100 %	30 %			
2CEL_Dec00	20	1.1	0.087	10.0	21	0.027	0.77	0.56	−0.26	10 %	97 %	−13.81		
2CEL_Jul02	20	11	0.094	13	28	0.0066	0.050	0.11	−0.03	65 %	95 %			
3CEL_Apr00	20	1.3	0.29	1.3	3.4	0.021	0.24	0.67	0.16	55 %	79 %			
3CEL_Jul02	20	7.1	0.25	7.1	14	0.067	2	3.0	0.64	10 %	100 %			
1_1CH_Oct01	14	24	31	24	113	0.19	0	11	−19.54	100 %	42 %	−0.5		
1_2CH_Oct01	20	3.0	27	3.0	63	0.40	0	21	−5.75	100 %	10 %			
Group-2														
1CH_Dec00	20	−7.1	0	−7.1	−53	0.16	20	12	−7.0			−10		
1CH_Apr00	20	1.9	0.016	1.9	4	0.0022	0.018	0.011	−0.02					
2CH_Dec00	20	2.2	0	2.2	7.8	0.00025	0	−0.00012	0.00013					
5CH_Apr00	20	2.2	0	2.2	7.8	0.00026	0	−0.00012	0.00013					
Group-3														
2CEL_Oct01	20	−2.1*		−2.1*		0.082		11	−0.01				3.9	11
14CEL_Jul02	20	−2.6*		−1.2*		0.016		0.27	−0.0032				3.7	0.27
16CEL_Dec00	20	−0.23*		−0.23*		0.0015		−0.047	0.013				−1.8	−0.060
Group-4														
5CEL_Apr00	10					0.0028		0.014	−0.01				−69	0.028
14CEL_Dec00	20					0.22		3.4	−0.13				10	3.6
14CEL_Oct01	20					0.0034		0.088	−0.01				2.9	0.10
Group-5														
16CEL_Jul02	20					0.011		0.096	0.02				6.1	0.072
16CEL_Oct01	20					0.0003		−0.000016	−0.0000073				0.83	−0.000011
7CH_Oct01	20					0.0029		0.13	−0.0071				2.6	0.14
8CH_Dec00	20					0.0015		0.006	−0.0056				0.85	0.012
3CEL_Dec00	20											−2.2		

R_{SD} is net sulfate depletion rate (mmol m^{-2} d^{-1} of SO_4^{2-}). F_M is methanogenesis rate (mmol m^{-2} d^{-1} of CH_4). F_{SR} is organoclastic sulfate reduction rate (mmol m^{-2} d^{-1} of SO_4^{2-}). R_{POC} is total POC mineralization rate (mmol m^{-2} d^{-1} of C). F_{AOM} is anaerobic oxidation of methane (mmol m^{-2} d^{-1} of CH_4). F_{MB} is gas dissolution (mmol m^{-2} d^{-1} of CH_4). $F_{methane\ (top)}$ is methane flux emitted to water column (mmol m^{-2} d^{-1} of CH_4). Negative values in $F_{methane\ (top)}$ represent methane enter sediments from water column. $F_{methane\ (bottom)}$ is methane flux from 20 cm to deep sediments (mmol m^{-2} d^{-1} of CH_4). Negative values in $F_{methane\ (bottom)}$ represent methane buried to deep sediments (> 20 cm). $F_{C_{organic}}$: organic carbon degradation rates (mmol m^{-2} d^{-1} of C). $F_{SO_4^{2-}}$ is net sulfate input rates (mmol m^{-2} d^{-1} of SO_4^{2-}) and F_{CH_4} is net methane production rates (mmol m^{-2} d^{-1} of CH_4) for cores in Group-3 to Group-5.

* Values were obtained from Eqs. (A5) and (A6) and were not included in Fig. 2.

BGD
12, 17913–17951, 2015

Table A1. Imposed and best-fit parameters in each core.

	T	S	P	$D_{m(SO_4^{2-})}$	$D_{m(CH_4)}$	$D_{m(SO_4^{2-}-dep)}$	L_{MB}	k_{SR}	k_{MB}	k_{SD}	k_{CH_4}	$k_{SO_4^{2-}}$
Group-1												
1CEL_Apr00	27.3	17.6	1.06	354	598	354	1.2	0.1	1	500		
1CEL_Dec00	22.2	16.4	1.06	367	523	367	1.3	0.1	0	400		
1CEL_Oct01	31.2	13.9	1.1	382	659	382	1.36	0.1	0.6	500		
1CEL_Jul02	30	21.1	1.01	374	640	374	1.1	0.1	0	500		
2CEL_Dec00	22	17.7	1.06	315	520	315	1.31	0.1	1.6	500		
2CEL_Jul02	28.7	20.8	1.01	364	619	364	1.12	0.1	0.1	500		
3CEL_Apr00	28.6	20.2	1.07	363	618	363	1.19	0.1	0.9	400		
3CEL_Jul02	30.4	18.2	1.01	377	646	377	1.09	0.1	50	500		
1_1CH_Oct01	29.8	32.1	1.01	372	636	372	1.1	0.1	0	500		
1_2CH_Oct01	29.8	32.1	1.01	372	636	372	1.1	0.1	0	500		
Group-2												
1CH_Dec00	25.2	24.8	1.05	318	526	318	1.23	0.1	500	100		
1CH_Apr00	26.3	39.4	1.09	347	583	347	1.25	0.1	0.03	500		
2CH_Dec00	23.9	27.5	1.08	329	547	329	1.29	0.1	0	100		
5CH_Apr00	29.6	38	1.04	382	659	382	1.14	0.1	0	500		
Group-3												
2CEL_Oct01	31.2	14.3	1.1	382	659						1000	500
14CEL_Jul02	31.5	27.4	1.01	385	663						1000	300
16CEL_Dec00	22.6	31.2	1.02	319	529						1000	300
Group-4												
5CEL_Apr00	26.5	21.1	1.06	348	586						1100	3000
14CEL_Dec00	23.5	31.1	1.06	326	541						1000	300
14CEL_Oct01	31.1	13.9	1.07	382	657						1000	500
Group-5												
16CEL_Jul02	30.3	30.5	1.01	376	644						600	300
16CEL_Oct01	29.7	28.2	1.06	319	529						1000	300
7CH_Oct01	29.6	31.3	1.01	371	633						500	300
8CH_Dec00	24.4	31.3	1.05	333	555						500	300

T is temperature (°C). S is salinity (–). P is pressure at sediment–water interface (bar). $D_{mSO_4^{2-}}$ is molecular diffusion coefficient for SO_4^{2-} ($cm^2\,yr^{-1}$). $D_{m(CH_4)}$ is molecular diffusion coefficient for CH_4 ($cm^2\,yr^{-1}$). $D_{m(SO_4^{2-}-dep)}$ is molecular diffusion coefficient for $SO_4^{2-}{}_{dep}$ ($cm^2\,yr^{-1}$). L_{MB} is equilibrium concentration for dissolved–gaseous CH_4 (mM). k_{SR} is sulfate half–saturation constant for POC degradation (k_{SR}, mM). k_{MB} is kinetic constant for methane gas dissolution (yr^{-1}). k_{SD} is kinetic constant for sulfate depletion rate (yr^{-1}). k_{CH_4} is kinetic constant for methane production rate (yr^{-1}). $k_{SO_4^{2-}}$ is kinetic constant for sulfate consumption rate (yr^{-1}).

BGD
12, 17913–17951, 2015

Table A2. Rate expressions applied in the differential equations.

Variable	Rates	Applied cores
SO_4^{2-}	$-R_{SR} - R_{AOM}$	Group-1 and Group-2
CH_4	$+R_M - R_{AOM} + R_{MB}$	Group-1 and Group-2
$SO_{4\ dep}^{2-}$	$+R_{SD}$	Group-1 and Group-2
$C_{organic}$	$+R_{C_{organic}}$	2CEL_Dec00, 3CEL_Dec00, 1CH_Oct01 and 1CH_Dec00
SO_4^{2-}	$+R_{SO_4^{2-}}$	Group-3, Group-4 and Group-5
CH_4	$+R_{CH_4}$	Group-3, Group-4 and Group-5

BGD
12, 17913–17951, 2015

Table A3. Boundary conditions used in the model.

	SO_4^{2-} (top)	CH_4 (top)	$SO_4^{2-}{}_{dep}$ (top)	SO_4^{2-} (bottom)	CH_4 (bottom)	$SO_4^{2-}{}_{dep}$ (bottom)	$C_{organic}$ (top)	$C_{organic}$ (bottom)	Unit
Group-1									
1CEL_Apr00	5	0	4.8	8.5	0.5	5.534			mM
1CEL_Dec00	15	0.16	−2.2	5	0.56	2			mM
1CEL_Oct01	15	0	−2.3	7.5	0.295	4.6			mM
1CEL_Jul02	15	0.1	2.5	7.8	0.35	5.368			mM
2CEL_Jul02	18	0.02	10^{-9}	18.5	0.035	−2			mM
3CEL_Apr00	6.5	0.25	6.7	3.5	0.825	5.766			mM
3CEL_Jul02	13.8	0.31	2	6.5	1.3	3.5			mM
1_1CH_Oct01	15.1	0	12.4	13.2	0.0295	12.03			mM
1_2CH_Oct01	12	0.01	16	10	1	14.641			mM
2CEL_Dec00	21	0.01	−6.4451	7.6	0.25	4.6			mM
Group-2									
1CH_Dec00	11.5	0.102	7.33	9.2	0.522	15.39			mM
1CH_Apr00	32	0.006	−0.0001	12.5	0.006	5.495			mM
2CH_Dec00	19.9	0.00213	1.19	7.96	2.23	4.8			mM
5CH_Apr00	31.7	0.00415	−0.001	29.1	0.0145	4.925			mM
Group-3									
2CEL_Oct01	5.0	0.511		7.88	0.734				mM
14CEL_Jul02	18.3	0.085		31.5	0.02				mM
16CEL_Dec00	8.8	0.038		8.81	0.025				mM
Group-4									
5CEL_Apr00	17	0.047		11.6	0.0275				mM
14CEL_Dec00	20.5	2.1		34.9	0				mM
14CEL_Oct01	20	0.01		33	0.012				mM
Group-5									
16CEL_Jul02	21	0		25.65	0.070				mM
16CEL_Oct01	23	0.00139		25.8	0.0015				mM
7CH_Oct01	20.5	0.00477		19.1	0.01				mM
8CH_Dec00	18.6	0		19	0.013				mM
2CEL_Dec00							0.06	4.64	wt %
3CEL_Dec00							3.12	3.78	wt %
1CH_Oct01							3.83	3.8	wt %
1CH_Dec00							3.7	6.97	wt %

BGD
12, 17913–17951, 2015

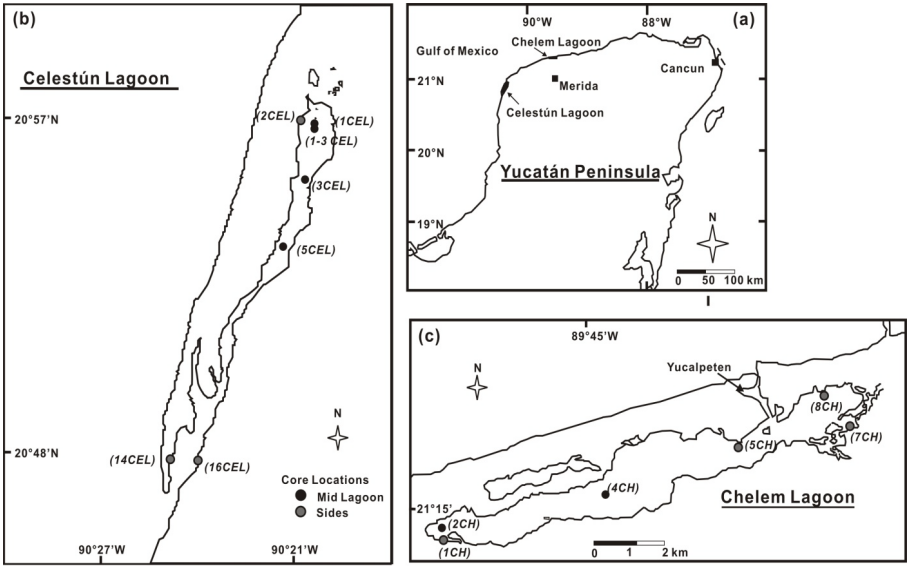

Figure 1. Maps of **(a)** the Yucatán Peninsula with lagoon locations, **(b)** Celestún Lagoon and **(c)** Chelem Lagoon showing the sampling stations (circles) of sediment cores.

BGD
12, 17913–17951, 2015

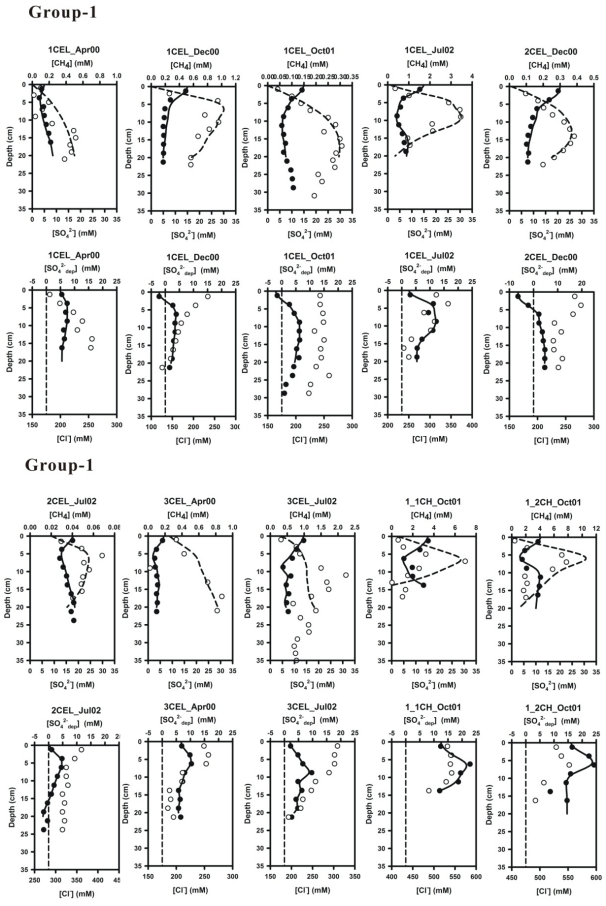

Figure 2.

BGD
12, 17913–17951, 2015

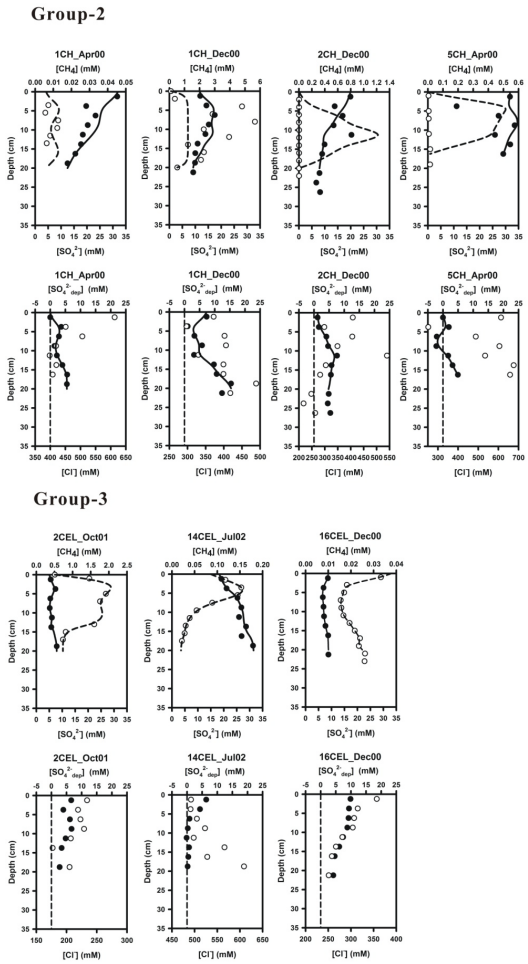

Figure 2.

BGD
12, 17913–17951, 2015

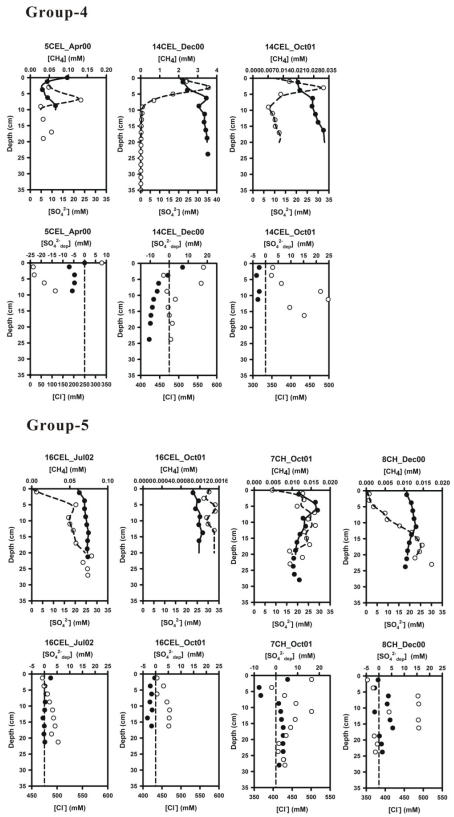

Figure 2. Depth profiles of modeled (lines) and measured/calculated (symbols) concentration of dissolved methane (dashed line; open circle), sulfate (solid line; solid circle) in the upper panel and sulfate depletion (solid line; solid circle), zero sulfate depletion (dashed line) and chloride (open circle) in the lower panel for each profile type (Groups 1–5, see text). Measured dissolved methane data from Chuang et al. (2015).

BGD
12, 17913–17951, 2015

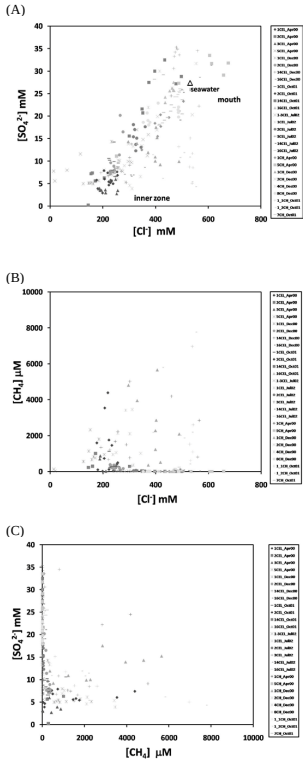

Figure 3. (a) Relationship between [Cl^-] and [SO_4^{2-}], **(b)** relationship between [Cl^-] and [CH_4] and **(c)** relationship between [CH_4] and [SO_4^{2-}] in porewater samples.

BGD
12, 17913–17951, 2015

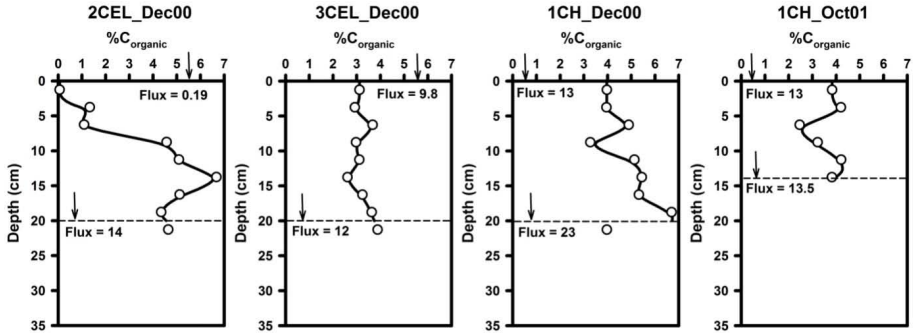

Figure 4. Depth profiles of modeled (curves) and measured/calculated (symbols) organic contents (in dry weight percent). The numbers represent organic matter deposition flux from the water to the sediment surface and burial flux from 20 cm to deeper depth (in mmol C m^{-2} d^{-1}). Data of 3CEL_Dec00 from Gonneea et al. (2004).

BGD
12, 17913–17951, 2015

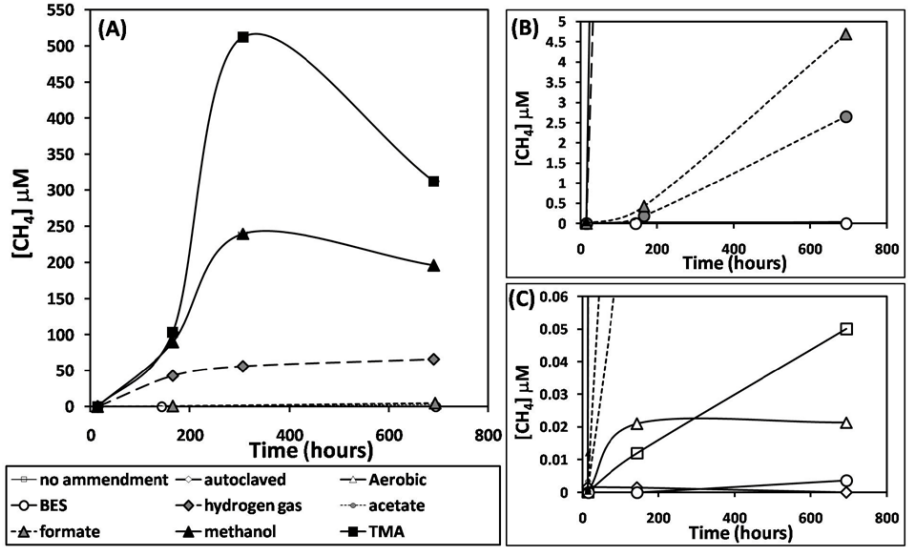

Figure 5. (a) Headspace CH_4 concentrations in sediment slurry incubations. **(b)** Expansion of **(a)**, showing results for acetate, formate, and controls. **(c)** Expansion of **(a)**, showing results for controls only. Error bars represent one standard deviation for triplicate sample bottles.

BGD
12, 17913–17951, 2015

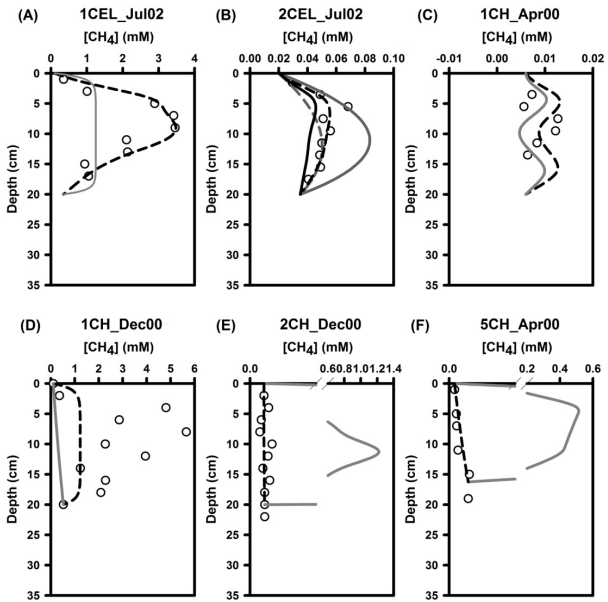

Figure 6. Sensitivity of methane concentrations for cores in Group-1 and Group-2 to the different processes: **(a)** $R_{CH_4} = -R_{AOM} + R_{MB}$ (gray solid line; $k_{MB} = 1000\,yr^{-1}$), **(b)** $R_{CH_4} = -R_{AOM} + R_{MB}$ (gray solid line; $k_{MB} = 0.5\,yr^{-1}$), $R_{CH_4} = -R_{AOM} + R_{MB}$ (gray dashed line; $k_{MB} = 0.2\,yr^{-1}$) and $R_{CH_4} = -R_{AOM} + R_M$ (black solid line), **(c)** $R_{CH_4} = -R_{AOM} + R_M$ (gray solid line), **(d)** $R_{CH_4} = -R_{AOM}$ (gray solid line), **(e)** $R_{CH_4} = -R_{AOM} + R_M$ (gray solid line), **(f)** $R_{CH_4} = -R_{AOM} + R_M$ (gray solid line). Black dashed curves denote the standard simulation results: **(a)** $R_{CH_4} = -R_{AOM} + R_M$ and **(b)** $R_{CH_4} = -R_{AOM} + R_{MB} + R_M$ ($k_{MB} = 0.1\,yr^{-1}$).

BGD
12, 17913–17951, 2015